

Deep Ultraviolet CMOS-Controlled Micro Light-Emitting Diode Array

Jonathan J. D. McKendry , Enyuan Xie , Jordan Hill , Hichem Zimi , Johannes Herrnsdorf , *Member, IEEE*, Erdan Gu , Robert K. Henderson , *Fellow, IEEE*, and Martin D. Dawson , *Fellow, IEEE*

Abstract—We report a Deep Ultraviolet (DUV) AlGaIn micro-light emitting diode (micro-LED) array driven by a matching array of electronic drivers implemented in Complementary Metal-Oxide-Semiconductor (CMOS) technology. This 40×10 pixel integrated device required improvements in micro-LED fabrication combined with control over the LED ground level in the custom designed CMOS chip. It allows each of the micro-LEDs, with a measured peak emission wavelength of 271 nm, to be addressed independently in continuous wave (CW) or nanosecond pulsed operation, with optical output powers and pulse energies per pixel of $80 \mu\text{W}$ and 0.2 pJ, respectively. Performance of this high-resolution electronically-driven array for multi-channel UV-C wireless communications is given as an example of its potentially wide-ranging uses.

Index Terms—Complementary metal-oxide-semiconductor (CMOS), GaN, AlGaIn, microdisplays, micro-light-emitting diodes (micro-LEDs), ultraviolet sources.

I. INTRODUCTION

ALGAN light-emitting diodes (LEDs) operating at short UV wavelengths, particularly in the UV-B (280–320 nm) and UV-C (200–280 nm) bands, are emerging as important sources for a wide variety of areas such as sterilization, phototherapy, photolithography, time-resolved fluorescence lifetime measurements, sensing, and optical communications [1]. The majority of such devices are in conventional ‘broad area’ format (active area ~ 0.1 – 1 mm^2) but recently various research groups, including our own, have demonstrated UV-B and UV-C ‘micro-LEDs’ where the pixel dimensions are $< 100 \mu\text{m}$ [2].

Micro-LEDs have been receiving great attention at visible wavelengths as a novel electronic visual display technology, but

extensive work (again, mostly at visible wavelengths) has also shown the advantages of these devices in digital light projection systems offering a high degree of spatio-temporal control, high modulation bandwidth, short (nanosecond) optical pulses, reduced self-heating and high output optical power densities, supporting a broad range of applications including biomedical sensing, optogenetics, visual and augmented reality, navigation and positioning systems, and high-speed optical wireless communications [3], [4].

The UV-B and UV-C micro-LED demonstrations to date have typically shown only single pixel operation [2], [5], [6], [7], [8], [9], [10], or a small number of pixels connected together in parallel [11], whereas the digital light projection applications highlighted above necessitate development of electronically interfaced high density arrays of micro-LED pixels. While CMOS (Complementary Metal-Oxide-Semiconductor) controlled micro-LED arrays with visible emission have been reported widely at longer wavelengths [12], [13], [14], there has thus far been no demonstration of UV-B or UV-C micro-LED arrays with fully-integrated electronic spatio-temporal control. UV micro-LEDs have significantly higher operating voltages than their visible-emitting counterparts, due to their intrinsically higher bandgap energy and issues owing to the lack of low-resistivity p-contacts and conductive p-type AlGaIn layers [1], making integration with low-voltage electronic technology such as CMOS challenging.

In this work we directly address this challenge. We describe progress in reducing the operating voltage of Deep UV (DUV) micro-LEDs and subsequent integration of a fully independently addressable 40×10 micro-LED array, with individual pixel dimensions of $80 \times 80 \mu\text{m}^2$, onto a matching custom CMOS Active Matrix driver array. For the first time to our knowledge, full electronic control of a UV-C micro-LED array in an integrated device is demonstrated. Continuous wave (CW) output powers of up to $80 \mu\text{W}$ per pixel and nanosecond-regime optical output pulses (important, for example, in time-resolved fluorescence or ranging applications) have been achieved. As an example of the use of such CMOS-integrated UV-C arrays in the important area of data communications, error-free wireless data transmission using On-Off Keying is shown here at up to 200 Mb/s from a single pixel and 800 Mb/s with four pixels transmitting simultaneously. We note that the operation of these devices in the ‘solar blind’ region offers novel capabilities for optical communications. More widely, CMOS-integrated deep-UV micro-LED arrays are expected to be applicable in areas

Manuscript received 8 September 2023; revised 13 October 2023; accepted 2 November 2023. Date of publication 6 November 2023; date of current version 16 November 2023. This work was supported in part by the Engineering and Physical Sciences Research Council under Grants EP/P02744X/2 and EP/T00097X/1, and in part by Innovate U.K. under Grant 10005391. (Corresponding author: Jonathan J. D. McKendry.)

Jonathan J. D. McKendry, Enyuan Xie, Jordan Hill, Hichem Zimi, Johannes Herrnsdorf, Erdan Gu, and Martin D. Dawson are with the Institute of Photonics, Department of Physics, University of Strathclyde, G1 1RD Glasgow, U.K. (e-mail: jonathan.mckendry@strath.ac.uk; enyuan.xie@strath.ac.uk; jordan.hill@strath.ac.uk; hichem.zimi@strath.ac.uk; johannes.herrnsdorf@strath.ac.uk; erdan.gu@strath.ac.uk; m.dawson@strath.ac.uk).

Robert K. Henderson is with the School of Engineering, Joint Research Institute for Integrated Systems, Institute for Micro and Nano Systems, University of Edinburgh, EH9 3JL Edinburgh, U.K. (e-mail: robert.henderson@ed.ac.uk).

This article has supplementary downloadable material available at <https://doi.org/10.1109/JPHOT.2023.3330571>, provided by the authors.

Digital Object Identifier 10.1109/JPHOT.2023.3330571

including mask-free photolithography, digital optical chemistry, chip-scale integrated systems, and remote sensing and imaging of bio- and chemical hazards and greenhouse gases.

II. DEVICE DESIGN AND FABRICATION

A. Micro-LED Array

The active-matrix micro-LED array with a flip-chip configuration is fabricated from commercial AlGaIn-based DUV LED wafers grown on a 2" c-plane sapphire substrate with a nominal peak emission wavelength ~ 280 nm. The detailed epitaxial structure of this wafer can be found in our previous work [15]. The resulting micro-LED array comprises 40×10 square-shaped micro-LED pixels, each $80 \times 80 \mu\text{m}^2$ in size, on a $100 \mu\text{m}$ center-to-center pitch between two adjacent pixels. The micro-LED pixels in this array are individually anode-controlled and have a shared cathode. Compared with the fabrication process for the visible-light active-matrix micro-LED array we demonstrated previously [16], an optimized metal contact specific to n-type AlGaIn is here employed for this DUV array. The metallization scheme of Ti/Al/Ti/Au followed by a high temperature annealing was developed as the Ohmic contact to highly n-doped AlGaIn to guarantee the low specific contact resistivity and, in turn, low turn-on voltage of the DUV micro-LED elements. As a result of this optimization the turn-on voltage has been reduced from 13 V that we reported previously for UV-C micro-LEDs [15], to around 7 V, as will be shown below in Section III-A.

B. CMOS Active Matrix Array

A detailed description of the design of the CMOS driver array and subsequent integration with longer wavelength micro-LED arrays has been reported in our previous work [17], but the features pertinent to this work are summarized as follows.

The CMOS driver chip was fabricated in a 5 V, $0.35 \mu\text{m}$ process. The chip comprises a 40×10 array of (400) individually-addressable drivers, with electrical contacts in a matching layout to that of the micro-LED array described above. Following fabrication of the CMOS and UV-C micro-LED dies, they were then integrated using a flip-chip bonding process whereby Au bumps connect the individual micro-LED anodes and the shared cathode to the CMOS supply voltages LED_VDD and LED_GND, respectively, as shown in Fig. 1(a). Direct integration of micro-LED and driver avoids the need for long metal tracks, wirebonds and packaging between micro-LED and driver that would otherwise contribute excess parasitic capacitance, inhibiting fast switching of the micro-LED output.

A micrograph image showing five active pixels driven in Continuous Wave (CW) mode by the fully assembled device is shown above in Fig. 1(b). A link to a supplementary video demonstrating live pattern display from this device is provided separately in the footnotes on page 1.

A simplified circuit diagram of an individual micro-LED driver element is shown in Fig. 1(c). Here LED_VDD can be varied from 0 to 5 V. However, due to the high turn-on voltage

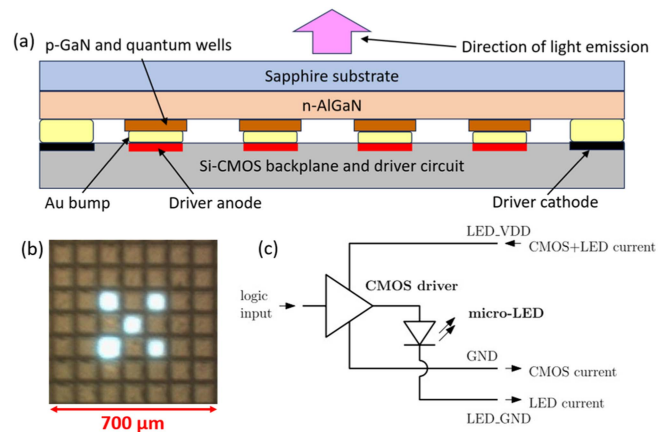


Fig. 1. (a) Cross section schematic showing flip-chip integration of the micro-LEDs and CMOS dies (not to scale), (b) enlarged plan view image showing 5 representative UV-C pixels in CMOS-driven operation and (c) simplified circuit diagram of a single micro-LED driver element.

of UV-C micro-LEDs, this is insufficient to drive these micro-LEDs. To increase the micro-LED bias voltage, LED_GND is separated from the global ground supply (GND) that supplies the rest of the CMOS logic. By applying a negative voltage (down to -3 V) a total bias voltage across the micro-LEDs of 8 V can be achieved allowing successful driving. A maximum drive current of ~ 300 mA can be supplied by each driver element.

The driver elements can be operated in a continuous wave (CW) or pulsed mode. For the latter, nanosecond electrical pulses can be generated on the CMOS driver chip and used to optically pulse the micro-LEDs, or alternatively the drivers can be driven by an external logic input signal. These short pulses are achieved using an inverter-based delay line. Pulse repetition rates exceeding 100 MHz are possible, triggered by an external clock signal. The CW and pulsed performance are described in the subsequent section. Grayscale control of the micro-LED emission is not possible from this device, however it would be possible with a different CMOS design adapted to UV-C operation, as illustrated by our recent demonstration of a blue-emitting CMOS-controlled micro-LED array with 128×128 pixels, 5 bit grayscale control, and a maximum frame update rate of 0.5 million frames per second [18].

III. DEVICE CHARACTERIZATION

A. Electrical Characteristics and Output Power

Fig. 2 shows the Voltage vs. Current (V-I) and Light Output Power vs. Current (L-I) plots for a representative single CMOS-driven UV-C micro-LED pixel. It can be seen that the micro-LED conducts < 0.25 mA for a forward bias of ≈ 6 V. This compares to the turn-on voltage of a UV-C micro-LED we reported previously in [15] with a turn-on voltage exceeding 10 V, well beyond the maximum 8 V that can be supplied by the CMOS drivers, highlighting the importance of the improved V-I characteristics shown here and also the importance of being able to shift LED_GND below the global CMOS GND, to increase the forward bias to the micro-LEDs beyond 5 V. This improved

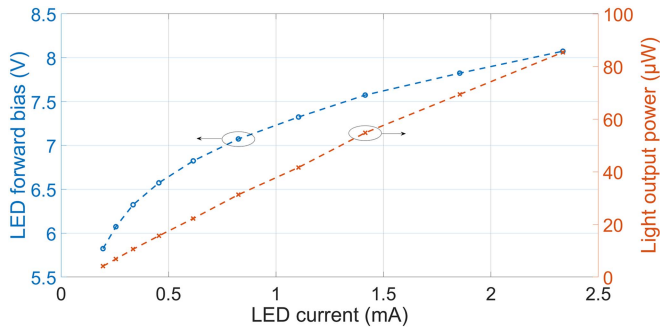


Fig. 2. Voltage (blue plot) and optical power (orange) versus current for a single CMOS-controlled UV-C micro-LED pixel.

V-I is at least comparable to the best performance reported by Yu et al. [19], and a significant improvement on I-Vs reported elsewhere, including in our own previous work [5], [6], [7], [8], [15].

A maximum optical output power of $\approx 80 \mu\text{W}$ (measured by a calibrated photodiode in close proximity to the device rather than using an integrating sphere, to capture the through-sapphire-substrate ‘directed output’) was obtained from a single pixel operating in continuous wave (CW) mode. This is limited by the voltage drive available from the CMOS, which limits the micro-LED bias current and thus in turn the optical output power. Based on measurements on such UV-C micro-LEDs prior to CMOS integration, and in reference to Fig. 2, without any constraints on the drive voltage such a micro-LED pixel should be able to source approximately several tens of mA and provide $>1 \text{ mW}$ of optical power. This, however, would require a forward bias $>11 \text{ V}$, beyond the 8 V currently available from the CMOS driver. Therefore, the output power of a DUV CMOS micro-LED array could be improved in future by further refining the micro-LED V-I characteristics and/or increasing the available drive voltage from the CMOS array. The corresponding External Quantum Efficiency of the micro-LEDs at maximum bias is approximately 0.75% . While this is low compared to visible LEDs, it is typical for a UVC LED emitting at 280 nm [1].

B. Electroluminescence (EL) Spectra

The EL spectra from a single representative pixel were measured using a spectrometer (Avantes Avaspec-2048) as a function of bias. The resulting EL spectrum when $\text{LED_VDD} = 5 \text{ V}$ and $\text{LED_GND} = -3 \text{ V}$ is shown in Fig. 3. The EL peaks at approximately 271 nm . The inset shown in Fig. 3 shows the same spectrum on a log scale, with very weak emission observed in the visible region of the spectrum. This weak visible emission explains why these UV-C micro-LEDs are visible in the optical micrograph shown in Fig. 1(b).

C. Nanosecond Optical Pulses

Nanosecond optical pulses from DUV LEDs have applications in areas including optical wireless communications (Pulse Position Modulation, for example), stand-off gas sensing, and

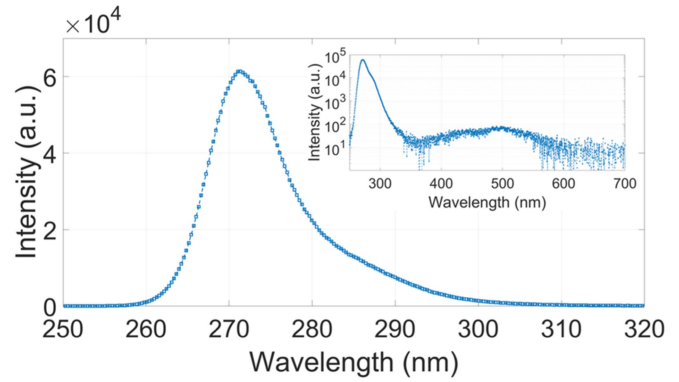


Fig. 3. CW EL spectrum from a single pixel with a total forward bias of 8 V (LED_VDD and $\text{LED_GND} = 5 \text{ V}$ and -3 V , respectively). Inset figure shows the same spectrum on a vertical log scale, showing weak secondary emission in the visible (c.f. Fig. 1(b)).

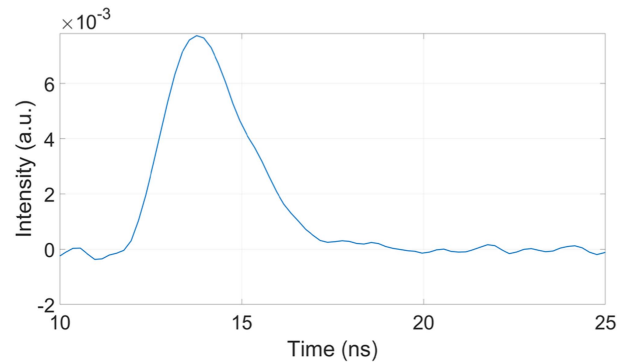


Fig. 4. Single micro-LED optical output pulse. FWHM = 2.6 ns . Total micro-LED bias = 8.5 V .

time-resolved fluorescence lifetime measurements, see e.g., [2]. As such, the nanosecond optical pulse characteristics of this device were important to measure.

In order to obtain the shortest optical output pulses to demonstrate the pulsed capability of the device, electrical pulses generated on-chip by the CMOS drivers were used. The corresponding optical output pulse was measured using a photomultiplier tube (PMT) with an instrument rise and fall time of 0.78 ns . Pulses of 2.6 ns full width half maximum (FWHM) were measured, a typical pulse measured from a single active micro-LED pixel being shown in Fig. 4.

The corresponding optical pulse energy and peak power output were measured by repetitively pulsing the pixel at a repetition rate of 10 MHz . The average optical power was then measured by placing a calibrated photodiode in close proximity to the pixel. From this, the average energy per pulse and corresponding peak power density were estimated to be 0.2 pJ and 1.18 W/cm^2 , respectively. An external 10 MHz digital signal was also used to pulse the same micro-LED with a pulse width of 40 ns , for which an average energy per pulse and corresponding peak power density were found to be 2 pJ and 0.78 W/cm^2 , respectively.

For comparison, we previously reported a $72 \mu\text{m}$ diameter micro-LED with peak wavelength of 370 nm as having a pulse energy and peak power density of 17.2 pJ and 10.56 W/cm^2 , respectively, for a 40 ns optical pulse [16].

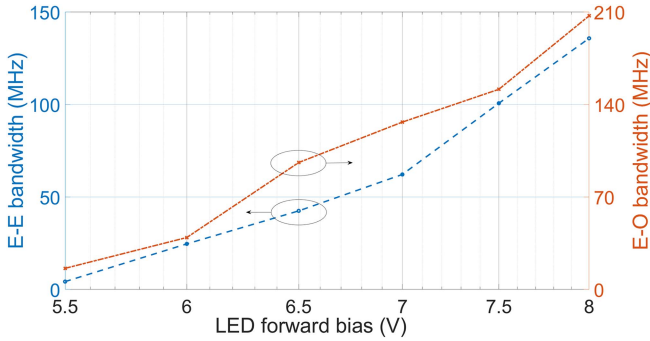


Fig. 5. Electrical-to-electrical (blue circles) and electrical-to-optical (orange crosses) bandwidths of a single micro-LED as a function of forward bias.

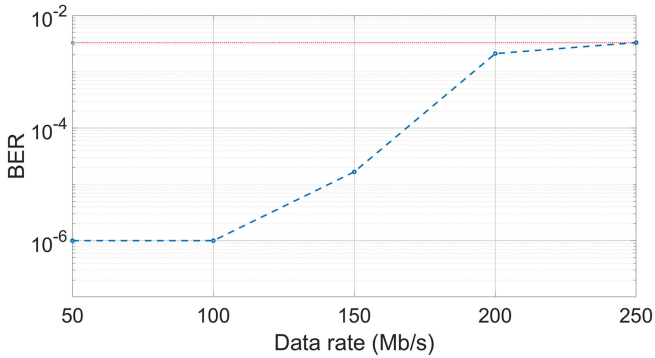


Fig. 6. Bit-error rate (BER) versus on-off keying data rate. Micro-LED bias 8 V. Red dashed line shows 3.3×10^{-3} ‘error free’ forward error correction limit. BERs at 50 and 100 Mb/s are $< 1 \times 10^{-6}$.

D. Single Channel Optical Wireless Communication

To illustrate the capacity of the chip to transmit Mb/s wireless optical data as one demonstration of its use, back-to-back measurements of the pixel frequency response and On-Off Keying (OOK) data transmission were obtained. In this configuration a CMOS logic-compatible digital signal was used to modulate a single pixel with a chirped square wave (for the frequency response) or a $2^7 - 1$ bit Pseudo-Random Bit Sequence (PRBS, for OOK transmission). The optical output was imaged onto a 1GHz bandwidth avalanche photodiode (Hamamatsu C5668 8867) in both cases.

The modulation bandwidth versus micro-LED forward bias is shown in Fig. 5. The Electrical-to-Electrical (E-E) and Electrical-to-Optical (E-O) modulation bandwidth are defined as the frequency at which the received electrical or optical powers, respectively, are -3dB lower than measured at low frequency. As observed in our previous work, the modulation bandwidth gradually increases with bias, which is attributed to an increase in the active region carrier density and corresponding decrease in carrier recombination time [16]. CMOS-limited E-O and E-E bandwidths of approximately 210 and 140 MHz, respectively, are observed.

Fig. 6 shows the Bit-Error Rate versus OOK data rate for a single micro-LED with a forward bias of 8 V. The red horizontal line represents the 3.8×10^{-3} limit at which Forward Error

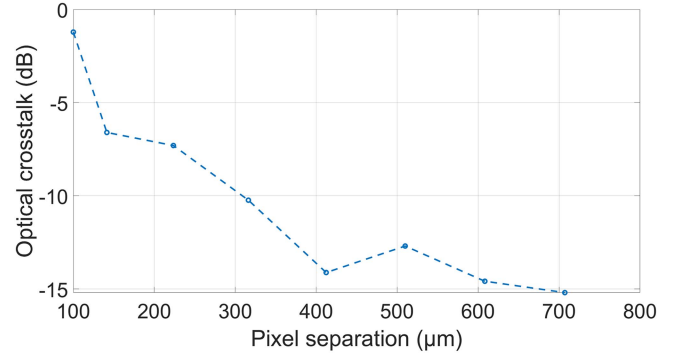


Fig. 7. Optical crosstalk versus pixel-to-pixel separation.

Correction (FEC) with a 7% overhead can be used to obtain ‘error free’ transmission. As can be seen in Fig. 6, error-free transmission is obtained at rates up to 200 Mb/s. While data rates exceeding 1 Gb/s have been demonstrated from single UV-C micro-LEDs by ourselves and others [2], [15], those demonstrations utilized more complex modulation schemes than OOK. In the following section we demonstrate how the aggregate data rate from this chip can be increased by implementing Multiple-Input Multiple-Output (MIMO) to transmit distinct data streams simultaneously from multiple CMOS-controlled micro-LED pixels.

E. Multi Channel Optical Wireless Communication

To expand upon the single-channel OOK demonstration, multi-channel transmission was also shown to illustrate how the arrayed nature of the CMOS-controlled micro-LED array can be exploited to further increase the wireless data rate. In this demonstration four micro-LED pixels were activated on the array. Following a similar approach to that we reported in [20], each micro-LED was modulated independently using the CMOS driver array’s ability to modulate each column of drivers with a separate input signal. An arbitrary waveform generator (AWG) with four output channels (Liquid Instruments “Moku Pro”) was used to provide independent $2^7 - 1$ long PRBS patterns, each at the same bit rate, separately to each of the corresponding column inputs.

Due to the Lambertian emission profile from the micro-LEDs, there exists optical crosstalk between micro-LEDs, whereby optical signals from one MIMO channel overlap with the optical path of neighboring channels. In future, this could be mitigated by the integration of micro-optics with the micro-LEDs. For this device, the optical crosstalk between pixels as a function of pixel separation was measured by aligning the transmission optics and receiver to one micro-LED (“Channel 1”). This pixel was then switched off, and without changing the optical alignment neighboring pixels were switched on one by one with increasing separation from Channel 1. The amplitude of the received signal when each of these neighboring pixels was active allowed the crosstalk as a function of pixel separation to be estimated. As can be seen in Fig. 7, beyond a separation of about 400 μm the crosstalk is reduced to around -14 dB. Based on this result,

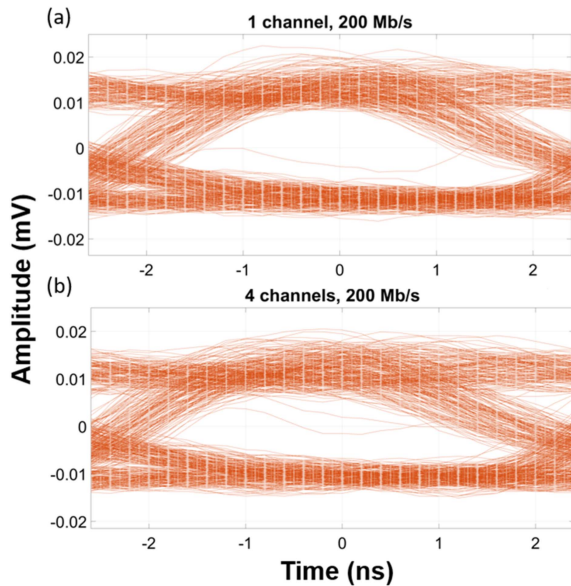


Fig. 8. Eye diagrams recorded at 200 Mb/s for channel 1 when (a) one and (b) four channels were active.

when choosing the pixel addresses to use for the multi-channel demonstration, a pixel-to-pixel separation of $1000\ \mu\text{m}$ was chosen to minimize the optical crosstalk between channels.

For the multi-channel data transmission, the transmission optics and receiver avalanche photodiode (APD) were aligned to one channel at a time. The received signal was then recorded at various data rates when one, two, three or four channels were active at once. The limit of four channels was set by the limited channels available from the AWG, but in principle all ten columns in the array could be modulated simultaneously. Fig. 8 shows eye diagrams recorded at 200 Mb/s with the receiver aligned to the micro-LED designated Channel 1, when either one or four channels are active. An open eye diagram is observed even with four channels active simultaneously.

The corresponding bit-error rates were calculated in MATLAB by decoding the received signal for each set of conditions and comparing the decoded bitstream to the original PRBS transmitted from the channel in question (in this case, Channel 1). From Fig. 6 the BER at 200 Mb/s for a single channel was estimated to be 2.1×10^{-3} . When four channels were active this increased slightly to 3.4×10^{-3} , which is still lower than the 3.8×10^{-3} FEC threshold for ‘error free’ transmission. Were extra receivers to be added to make a full MIMO system, this demonstrates how the data rate could be scaled by increasing the number of parallel channels, scaling from 200 to 800 Mb/s in this example.

The degradation of the BER with increasing channel count can be partially attributed to the aforementioned optical crosstalk. In addition to this there is electrical crosstalk between pixels caused by parasitic resistance and voltage drops in the CMOS and micro-LED dies, as we described previously in [20]. In future, optical and electrical crosstalk could be further mitigated by careful optimization of the transmitter optics and reducing

parasitic resistances on the dies through careful layout of metal contact grids, respectively.

IV. CONCLUSION

A micro-LED array emitting UV-C light, with a peak wavelength around 270 nm, has been demonstrated fully integrated with a dedicated array of individual pixel drivers implemented in CMOS. To the best of our knowledge, this is the first time that a UV-C micro-LED array has been monolithically integrated with an electronic driver that allows for full control of the spatio-temporal properties of the output.

The array comprises a 40×10 array of $80 \times 80\ \mu\text{m}^2$ pixels on a $100\ \mu\text{m}$ center-to-center pitch. Pixels can be operated in CW or nanosecond pulsed mode. A maximum CW output power of $80\ \mu\text{W}$ per pixel was demonstrated, and in pulsed mode optical pulse durations and energies of 2.6 ns and 0.2 pJ, respectively. To demonstrate one possible application of this device, CMOS-driven modulation bandwidths from single pixels exceeding 200 MHz are shown, alongside error-free optical wireless data transmission up to 200 Mb/s from a single pixel, scaling to a potential 800 Mb/s using four.

Such low size, weight and power (SWaP) arrayed UV-C devices should find a wide range of uses in applications such as optical communications, photolithography, lab-on-chip systems, imaging and remote sensing. Future optimization of the UV-C micro-LEDs’ electrical characteristics and/or the drive voltages available from the CMOS drivers are expected to enable an order of magnitude improvement in the optical powers and pulse energies shown here.

REFERENCES

- [1] H. Amano et al., “The 2020 UV emitter roadmap,” *J. Phys. D: Appl. Phys.*, vol. 53, no. 50, 2020, Art. no. 503001, doi: [10.1088/1361-6463/aba64c](https://doi.org/10.1088/1361-6463/aba64c).
- [2] P. Tian et al., “AlGaIn ultraviolet micro-LEDs,” *IEEE J. Quantum Electron.*, vol. 58, no. 4, Aug. 2022, Art. no. 3300214, doi: [10.1109/JQE.2022.3159854](https://doi.org/10.1109/JQE.2022.3159854).
- [3] H. X. Jiang and J. Y. Lin, Eds., “Micro LEDs,” in *Semiconductors and Semimetals*, New York, USA: Elsevier Sci., vol. 106, 2021, ch. 1, pp. 1–56.
- [4] J. Herrnsdorf, M. D. Dawson, and M. J. Strain, “Positioning and data broadcasting using illumination pattern sequences displayed by LED arrays,” *IEEE Trans. Commun.*, vol. 66, no. 11, pp. 5582–5592, Nov. 2018, doi: [10.1109/TCOMM.2018.2850892](https://doi.org/10.1109/TCOMM.2018.2850892).
- [5] S. Zhu et al., “2 Gbps free-space ultraviolet-C communication based on a high-bandwidth micro-LED achieved with pre-equalization,” *Opt. Lett.*, vol. 46, no. 9, pp. 2147–2150, 2021.
- [6] Z. Qian et al., “Size-dependent UV-C communication performance of AlGaIn micro-LEDs and LEDs,” *J. Lightw. Technol.*, vol. 40, no. 22, pp. 7289–7296, Nov. 2022, doi: [10.1109/JLT.2022.3202182](https://doi.org/10.1109/JLT.2022.3202182).
- [7] Y. Yao et al., “Size dependent characteristics of AlGaIn-based deep ultraviolet micro-light-emitting-diodes,” *Appl. Phys. Exp.*, vol. 15, no. 6, May 2022, Art. no. 064003, doi: [10.35848/1882-0786/ac6da0](https://doi.org/10.35848/1882-0786/ac6da0).
- [8] F. Feng et al., “AlGaIn-based deep-UV micro-LED array for quantum dots converted display with ultra-wide color gamut,” *IEEE Electron Device Lett.*, vol. 43, no. 1, pp. 60–63, Jan. 2022, doi: [10.1109/LED.2021.3130750](https://doi.org/10.1109/LED.2021.3130750).
- [9] S. Zhang et al., “Plasmon-enhanced deep ultraviolet micro-LED arrays for solar-blind communications,” *Opt. Lett.*, vol. 48, no. 15, pp. 3841–3844, Aug. 2023, doi: [10.1364/OL.496397](https://doi.org/10.1364/OL.496397).
- [10] J. Rass et al., “Enhanced light extraction efficiency of far-ultraviolet-C LEDs by micro-LED array design,” *Appl. Phys. Lett.*, vol. 122, no. 26, 2023, Art. no. 263508, doi: [10.1063/5.0154031](https://doi.org/10.1063/5.0154031).

- [11] M. H. Memon et al., "Quantum dots integrated deep-ultraviolet micro-LED array toward solar-blind and visible light dual-band optical communication," *IEEE Electron Device Lett.*, vol. 44, no. 3, pp. 472–475, Mar. 2023, doi: [10.1109/LED.2023.3239393](https://doi.org/10.1109/LED.2023.3239393).
- [12] X. Zhang et al., "Active matrix monolithic LED micro-display using GaN-on-Si epilayers," *IEEE Photon. Technol. Lett.*, vol. 31, no. 11, pp. 865–868, Jun. 2019, doi: [10.1109/lpt.2019.2910729](https://doi.org/10.1109/lpt.2019.2910729).
- [13] J. Day, J. Li, D. Y. C. Lie, C. Bradford, J. Y. Lin, and H. X. Jiang, "III-nitride full-scale high-resolution microdisplays," *Appl. Phys. Lett.*, vol. 99, no. 3, 2011, Art. no. 031116, doi: [10.1063/1.3615679](https://doi.org/10.1063/1.3615679).
- [14] X. Li, B. Hussain, J. Kang, H. S. Kwok, and C. P. Yue, "Smart μ LED display-VLC system with a PD-based/camera-based receiver for NFC applications," *IEEE Photon. J.*, vol. 11, no. 1, Feb. 2019, Art. no. 7901008, doi: [10.1109/JPHOT.2019.2892948](https://doi.org/10.1109/JPHOT.2019.2892948).
- [15] X. He et al., "1 Gbps free-space deep-ultraviolet communications based on III-nitride micro-LEDs emitting at 262 nm," *Photon. Res.*, vol. 7, no. 7, pp. B41–B41, 2019, doi: [10.1364/PRJ.7.000B41](https://doi.org/10.1364/PRJ.7.000B41).
- [16] J. J. D. McKendry et al., "Individually addressable AlInGaN micro-LED arrays with CMOS control and subnanosecond output pulses," *IEEE Photon. Technol. Lett.*, vol. 21, no. 12, pp. 811–813, Jun. 2009, doi: [10.1109/LPT.2009.2019114](https://doi.org/10.1109/LPT.2009.2019114).
- [17] J. Herrnsdorf et al., "Active-matrix GaN micro light-emitting diode display with unprecedented brightness," *IEEE Trans. Electron Devices*, vol. 62, no. 6, pp. 1918–1925, Jun. 2015.
- [18] N. Bani Hassan et al., "Ultrahigh frame rate digital light projector using chip-scale LED-on-CMOS technology," *Photon. Res.*, vol. 10, no. 10, pp. 2434–2446, Oct. 2022, doi: [10.1364/PRJ.455574](https://doi.org/10.1364/PRJ.455574).
- [19] H. Yu et al., "AlGaIn-based deep ultraviolet micro-LED emitting at 275 nm," *Opt. Lett.*, vol. 46, no. 13, pp. 3271–3274, Jul. 2021, doi: [10.1364/OL.431933](https://doi.org/10.1364/OL.431933).
- [20] S. Zhang et al., "1.5 Gbit/s multi-channel visible light communications using CMOS-controlled GaN-based LEDs," *J. Lightw. Technol.*, vol. 31, no. 8, pp. 1211–1216, Apr. 2013, doi: [10.1109/JLT.2013.2246138](https://doi.org/10.1109/JLT.2013.2246138).